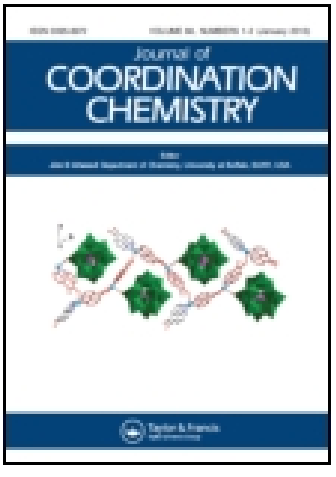

Journal of Coordination Chemistry
Publication details, including instructions for authors and subscription information:
http://www.tandfonline.com/loi/gcoo20

Assembly of three supramolecular compounds based on $[P_2Mo_5O_{23}]^{6-}$ and Ni(II) complexes

Li Song[a], Kai Yu[a], Zhanhua Su[a], Chunxiao Wang[a], Chunmei Wang[a] & Baibin Zhou[a]

[a] Key Laboratory of synthesis of functional materials and green catalysis, Colleges of Heilongjiang Province, Harbin Normal University, Harbin, PR China

Accepted author version posted online: 17 Feb 2014.Published online: 17 Mar 2014.

To cite this article: Li Song, Kai Yu, Zhanhua Su, Chunxiao Wang, Chunmei Wang & Baibin Zhou (2014) Assembly of three supramolecular compounds based on $[P_2Mo_5O_{23}]^{6-}$ and Ni(II) complexes, Journal of Coordination Chemistry, 67:3, 522-532, DOI: 10.1080/00958972.2014.894994

To link to this article: http://dx.doi.org/10.1080/00958972.2014.894994

Journal of Coordination Chemistry, 2014
Vol. 67, No. 3, 522–532, http://dx.doi.org/10.1080/00958972.2014.894994

Assembly of three supramolecular compounds based on $[P_2Mo_5O_{23}]^{6-}$ and Ni(II) complexes

LI SONG, KAI YU*, ZHANHUA SU, CHUNXIAO WANG, CHUNMEI WANG and BAIBIN ZHOU*

Key Laboratory of synthesis of functional materials and green catalysis, Colleges of Heilongjiang Province, Harbin Normal University, Harbin, PR China

(*Received 22 August 2013; accepted 1 February 2014*)

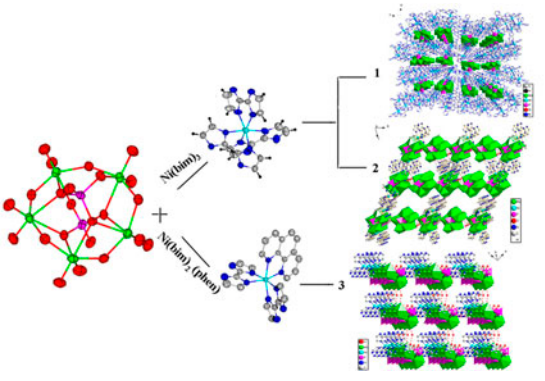

Three 3-D supramolecular networks constructed from weak interactions among free Ni(II) complex, water molecule, and oxygen atoms of $[P_2Mo_5O_{23}]^{6-}$ polyanions have been synthesized. The compounds display good electrocatalytic activity to reduce hydrogen peroxide and intensive fluorescent properties in the solution at room temperature.

Three supramolecular compounds based on $[P_2Mo_5O_{23}]^{6-}$ and Ni(II)–bim, $[Ni(bim)_3]_3[P_2Mo_5O_{23}]\cdot 2H_2O$ (**1**), $[Ni(Hbim)(bim)_2]_4[P_2Mo_5O_{23}]_2\cdot 3H_2O$ (**2**), and $[Ni(bim)(Hbim)(phen)]_2[P_2Mo_5O_{23}]\cdot 7H_2O$ (**3**) (bim = 2,2′-biimidazole, phen = 1,10-phenanthroline), have been synthesized under hydrothermal conditions and characterized by elemental analysis, single-crystal X-ray diffraction, IR, and TG. All the compounds show 3-D supramolecular networks constructed from weak interactions among free Ni(II) complex, water, and oxygens of $[P_2Mo_5O_{23}]^{6-}$. Compound **3** represents the first supramolecular example integrating {Ni(bim)(Hbim)(phen)} with Strandberg-type phosphomolybdate. The compounds display good electrocatalytic activity to reduce hydrogen peroxide and intense fluorescence properties in solution at room temperature.

Keywords: Supramolecular compounds; $[P_2Mo_5O_{23}]^{6-}$ unit; Ni(II) complex; Electrocatalytic activity; Fluorescent properties

*Corresponding authors. Email: hlyukai188@163.com (K. Yu); zhou_bai_bin@163.com (B.B. Zhou)

1. Introduction

Polyoxometalates (POMs) have attracted attention in creating supramolecular assemblies due to their rich structural chemistry and widespread potential applications in catalysis, medicine, magnetism, materials, and photochemistry [1–5]. Supramolecular materials extend low-dimensional building blocks to high-dimensional networks through weak intermolecular interactions, including hydrogen bonding, π–π stacking, and weak van der Waals force. During the construction of POM-based supramolecular assemblies, one promising strategy is to build connections between the surface oxygens of POMs and various organic units or transition metal complexes by covalent bond and weak intermolecular interaction. Through such interactions, organic components can dramatically influence the microstructure and character of hybrid materials. Thus combination of metal/ligand/POM is a factor for design of POM-based supramolecular hybrids. Among POM building blocks, the Strandberg-type polyoxoanions have been employed as the appropriate candidates to incorporate transition metals and organic ligands into multi-dimensional topological architectures [6–14].

A large amount of organic–inorganic hybrids based on Strandberg-type polyoxoanions have been reported [15–23]; most of these studies focus on covalent hybrids. Supramolecular compounds based on these POMs are less common, because coordination of metal ions, steric hindrance of the ligands, and geometrical relations [24]; 1-, 2-, and even 3-D supramolecular architectures have been synthesized [25–28]. Hydrogen bonds which play an important role in formation of the overall configuration were neglected in most cases [29]. Supramolecular cements like O–H···O, N–H···O, C–H···O, and O–H···N hydrogen bonding interactions play crucial roles in crystal engineering of supramolecular assemblies [30–33]. It is relatively rare that Ni(II)-bim segments are linkers for construction of Strandberg-type supramolecular compounds by weak intermolecular interaction.

Based on the results of previous work [34, 35], three new P_2Mo_5-based supramolecular compounds, $[Ni(bim)_3]_3[P_2Mo_5O_{23}]\cdot 2H_2O$ (**1**), $[Ni(Hbim)(bim)_2]_4[P2Mo_5O_{23}]_2\cdot 3H_2O$ (**2**), and $[Ni(bim)(Hbim)(phen)]_2[P_2Mo_5O_{23}]\cdot 7H_2O$ (**3**), have been obtained through changing the stoichiometry and kind of ligands under hydrothermal conditions. Their electrochemical characteristics, electrocatalytic behavior, and fluorescent properties in the solid state at room temperature have been studied.

2. Experimental

2.1. *Materials and general procedures*

All reagents were purchased commercially and used without purification. Elemental analyses (C, H, and N) were performed on a Perkin–Elmer 2400 CHN Elemental Analyzer. P, Mo, and Ni analyses were performed on a PLASMA-SPEC (I) inductively coupled plasma-atomic emission spectrometer. IR spectra were recorded from 4000 to 400 cm^{-1} on an Alpha Centaurt FT-IR spectrometer with pressed KBr pellets. Thermogravimetric analyses were recorded in a dynamic nitrogen atmosphere with a heating rate of 10 °C/min using a Perkin–Elmer DTA 1700 differential thermal analyzer. A CHI600D electro-chemical workstation connected to a Digital-586 personal computer was used for control of the electrochemical measurements and for data collection. A conventional three-electrode system was used. The working electrode was a modified carbon paste electrode (CPE). A Ag/AgCl (3 M KCl) electrode was used as a reference electrode and a Pt wire as a counter electrode.

Fluorescence spectra were performed on a Hitachi F-4500 fluorescence/phosphorescence spectrophotometer with a 450 W xenon lamp as the excitation source.

2.2. *Synthesis of 1*

The synthesis of **1** was carried out under hydrothermal conditions. A mixture of $Na_2MoO_4{\cdot}2H_2O$ (0.134 g, 1 mM), NaH_2PO_4 (0.173 g, 2 mM), bim (0.234 g, 1.74 mM), and $Ni(NO_3)_2{\cdot}5H_2O$ (0.298 g, 1.05 mM) was dissolved in 10 mL of distilled water. The mixture was stirred for 30 min at room temperature and then heated in a 30 mL Teflon-lined stainless steel autoclave for 3 days at 160 °C. After slow cooling to room temperature, the solid product was washed with distilled water and blue crystals were isolated in 48% yield (based on Mo). Anal. $C_{54}H_{40}Mo_5N_{36}Ni_3O_{25}P_2$ found: C, 28.06; H, 1.69; N, 21.78; P, 2.63; Mo, 20.71; Ni, 7.59. Calcd: C, 28.06; H, 1.74; N, 21.82; P, 2.68; Mo, 20.75; Ni, 7.62.

2.3. *Synthesis of 2*

The synthesis of **2** was carried out under hydrothermal conditions. A mixture of $Na_2MoO_4{\cdot}2H_2O$ (0.3604 g, 1.5 mM), H_3PO_4 (0.6 mL, 8.85 mM), bim (0.067 g, 0.5 mM), and $NiSO_4{\cdot}5H_2O$ (0.1435 g, 0.75 mM) was dissolved in 20 mL of distilled water. The mixture was stirred for 30 min at room temperature and then heated in a 30 mL Teflon-lined stainless steel autoclave for 6 days at 160 °C. After slow cooling to room temperature, the solid product was washed with distilled water and blue crystals were isolated in 54% yield (based on Mo). Anal. $C_{72}H_{58}Mo_{10}N_{48}Ni_4O_{49}P_4$ found: C, 23.34; H, 1.53; N, 18.13; P, 3.32; Mo, 25.87; Ni, 6.31. Calcd: C, 23.39; H, 1.58; N, 18.19; P, 3.35; Mo, 25.95; Ni, 6.35.

2.4. *Synthesis of 3*

The synthesis of **3** was carried out under hydrothermal conditions. A mixture of $Na_2MoO_4{\cdot}2H_2O$ (0.7209 g, 3 mM), H_3PO_4 (0.6 mL, 8.85 mM), bim (0.1341 g, 1 mM), phen (0.15 g, 0.77 mM), and $NiSO_4{\cdot}5H_2O$ (0.2949 g, 1.05 mM) was dissolved in 20 mL of distilled water. The mixture was stirred for 30 min at room temperature and then heated in a 30 mL Teflon-lined stainless steel autoclave for 6 days at 160 °C. After slow cooling to room temperature, the solid product was washed with distilled water and then blue crystals were isolated in 65% yield (based on Mo). Anal. $C_{96}H_{94}Mo_{10}N_{40}Ni_4O_{59}P_4$ found: C, 28.27; H, 2.28; N, 13.71; P, 3.01; Mo, 23.52; Ni, 5.71. Calcd: C, 28.33; H, 2.33; N, 13.77; P, 3.04; Mo, 23.57; Ni, 5.77.

2.5. *Preparation of 1- to 3-CPEs*

Complexes **1**, **2**, and **3** modified the carbon paste electrodes and **1**–**3**-CPEs were fabricated as follows: 300 mg of graphite powder and 30 mg of complex were mixed and ground together by agate mortar and pestle to achieve a uniform mixture. To the mixture, three drops of Nujol were added with stirring. The homogenized mixture was packed into a glass tube with 3 mm inner diameter and the surface was pressed tightly onto weighing paper with a copper rod through the back. Electrical contact was established with a copper rod through the back of the electrode.

2.6. *X-ray crystallography*

The crystal data of **1–3** were collected on a Bruker SMART CCD diffractometer with Mo Kα radiation ($\lambda = 0.71073$ Å) at 293 K. The structures were solved by the direct methods and difference Fourier map with SHELXL-97 [36, 37] and refined by full-matrix least-squares on F^2. Anisotropic thermal parameters were used to refine non-hydrogen atoms. Hydrogens on C and N of the organic ligands were included in their calculated positions. Hydrogens attached to hydroxyl and lattice waters were found from the difference Fourier maps. A summary of crystal data and structure refinement for **1–3** is provided in table 1. Selected bond lengths and angles of **1–3** are listed in table S2.

3. Results and discussion

3.1. *Structure description*

X-ray diffraction analysis reveals that the structures of **1–3** are based on P_2Mo_5 cluster (figure 1). The polyoxoanion cluster $\{P_2Mo_5\}$ consists of a pentagonal ring formed by five distorted edge- and corner-sharing MoO_6 octahedra. Two $\{PO_4\}$ groups are capped above and below the Mo5 ring by sharing three oxygens with different MoO_6 units (shown in figure 1). The P–O distances are 1.507(3)–1.562(3) Å, 1.507(3)–1.572(4) Å, and 1.514(4)–1.566(5) Å for **1–3**, respectively. Relevant Mo–O distances are 1.685(3)–2.503(3) Å, 1.684 (4)–2.493(3) Å, and 1.685(4)–2.411(3) Å for **1–3**, respectively. All P–O and Mo–O bond lengths are in the normal ranges. Bond valence sum calculations indicate that all Mo and Ni ions in **1–3** are in +VI and +II oxidation states, respectively.

Table 1. Crystal data and structure refinement parameters for **1**, **2,** and **3**.

Compound	**1**	**2**	**3**
Formula	$C_{54}H_{40}Mo_5N_{36}Ni_3O_{25}P_2$	$C_{72}H_{58}Mo_{10}N_{48}Ni_4O_{49}P_4$	$C_{96}H_{94}Mo_{10}N_{40}Ni_4O_{59}P_4$
Mr	2310.93	3697.07	4070.16
Crystal size, mm^3	0.32 × 0.30 × 0.24	0.42 × 0.40 × 0.26	0.28 × 0.26 × 0.20
Crystal system	Orthorhombic	Triclinic	Triclinic
Space group	Pbca	P-1	P-1
a, Å	15.5334(7)	16.5703(6)	14.3433(8)
b, Å	26.5038(12)	16.8354(6)	16.0053(9)
c, Å	41.9154(19)	23.9503(9)	17.8043(10)
β, (°)	90	80.09	81.89
V ($Å^3$)	17256.3(14)	5960.1(4)	3403.1(3)
Z	8	2	1
D_{Calcd}, g cm^{-3}	2.728	2.062	1.988
μ(MoKα), cm^{-1}	1.469	1.789	1.580
F (0 0 0), e	9132	3628	2036
θ range, °	2.24–28.30	2.30–28.29	2.30–28.28
Reflections collected/unique/R_{int}	127688/21418/0.0362	48877/29497/0.0169	27556/16829/0.0170
Data/restraints/parameters	21352/0/1126	28505/6/1684	16198/30/961
R_1/wR_2 $[I \geq 2\sigma(I)]$[a]	0.0424/0.1228	0.0435/0.1025	0.0462/0.1129
$R(F)/wR(F^2)$[a] (all refl.)	0.0593/0.1348	0.0539/0.1103	0.0622/0.1249
GoF (F^2)[a]	1. 096	1.024	1.033
Δ*ρ*fin (max/min), e $Å^{-3}$	2.818/−0.570	2.337/−1.728	2.335/−1.574

[a]$R_1 = \sum||F_0| - |F_C||/\sum|F_0|$; $wR_2 = \sum[w(F_0^2 - F_C^2)^2]/\sum[w(F_0^2)^2]^{1/2}$, $w = [\sigma^2(F_0^2) + (0.484P)^2 + 24.2999P]^{-1}$, where $P = (\mathrm{Max}(F_0^2,0)+2F_C^2)/3$, GoF = $[\sum w(F_0^2 - F_C^2)^2/(n_{obs} - n_{param})]^{1/2}$.

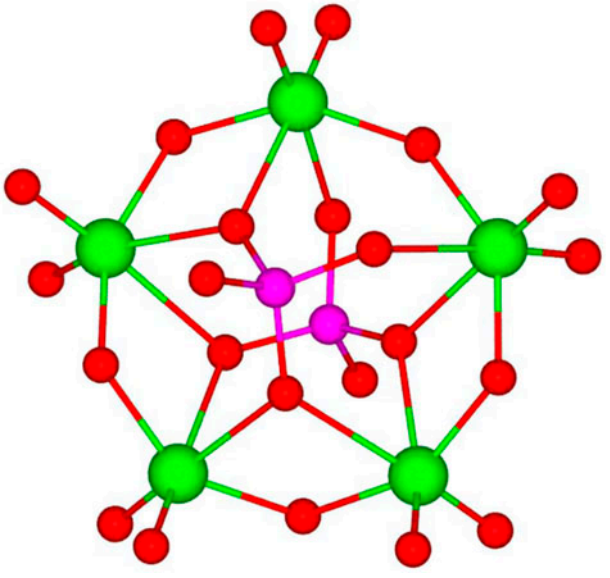

Figure 1. Ball–stick representation of the basic building unit of $[P_2Mo_5O_{23}]^{6-}$.

3.1.1. Structure description of 1. Single crystal X-ray diffraction analysis shows that the structure of **1** is composed of one $[P_2Mo_5O_{23}]$, three $[Ni(bim)_3]$ anions, and two lattice waters, as shown in figure S1 (see online supplemental material at http://dx.doi.org/10.1080/00958972.2014.894994). There are three kinds of crystallographically independent Ni^{2+} cations, which exhibit similar coordination environments in **1**. All Ni^{2+} cations are coordinated by six nitrogens from three different bim to form an octahedral geometry. The Ni–N distances are 2.053(4)–2.183(4) Å and N–Ni–N bond angles of **1** are 78.7(2)–171.65 (16)°. In the polyhedral and ball–stick representation of **1**, there exist hydrogen bonds (table S1). Two adjacent $[P_2Mo_5O_{23}]^{6-}$ anions are bonded by weak interactions between Ni $(bim)_3$, H_2O, and oxygens of polyanions to a dimer. The dimeric units are further linked by another H_2O to form infinite 1-D chains in ABAB mode via hydrogen bonds (O25···O7 3.128(9) Å shown in table S1) and supramolecular interaction (O25···O21 3.015 Å) (figure S2). The adjacent chains are further aggregated by $Ni(bim)_3$ and H_2O to yield a 2-D supramolecular layer in ABAB mode via supramolecular interaction (N21···O19 2.658 Å and N19···O3 2.962 Å) (figure 2). The 3-D supramolecular framework (figure S3) was generated by similar supramolecular interactions.

3.1.2. Structure description of 2. When we changed NaH_2PO_4 to H_3PO_4, **2** was obtained. Single crystal X-ray diffraction analysis show that the structure of **2** is composed of two $[P_2Mo_5O_{23}]$ clusters, four isolated $[Ni(Hbim)(bim)_2]$ anions, and two lattice waters (figure S4). There are four crystallographically independent Ni^{2+} cations, which exhibit similar coordination to those in **1**. Ni–N distances are 2.075(4)–2.154(4) Å and the N–Ni–N bond angles are 78.92(15)–172.41(15)°. In **2**, two crystallographically independent $[P_2Mo_5O_{23}]$ clusters are connected to form a dimer via weak supramolecular interactions (O46···O28 2.663 and O42···O39 2.894 Å). The dimeric units are further linked by H_2O to

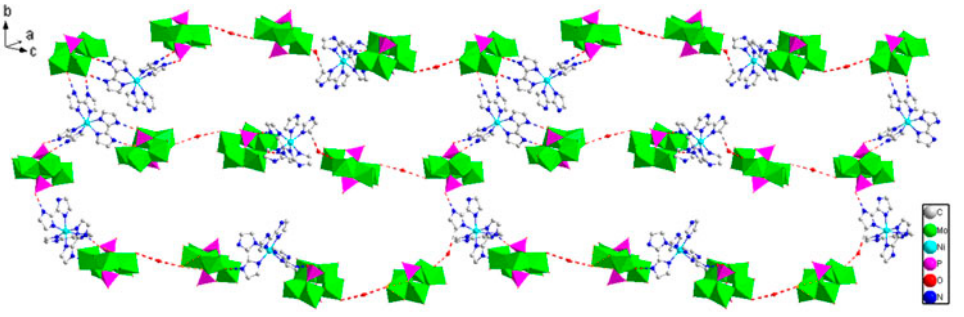

Figure 2. Polyhedral and ball–stick representation of the 2-D layers in **1**.

form 1-D chains via hydrogen bonds (O48···O17 2.944(7) and O48···O15 2.954(6) Å shown in table S1) (figure S5). In the packing arrangement, adjacent 1-D chains are parallel and linked to form a 2-D supramolecular layer via supramolecular interaction (N41···O35 2.994, N22···O24 2.784, N44···O34 2.987, and N38···O15 2.894) between terminal phosphate O of polyoxoanions and N of {Ni(Hbim)$(bim)_2$} (figure 3). Adjacent 2-D layers are further supported by similar supramolecular interactions to extend into a 3-D network structure (figure S6).

3.1.3. Structure description of 3. Single crystal X-ray diffraction analysis shows that **3** is composed of one $[P_2Mo_5O_{23}]$, two isolated [Ni(bim)(Hbim)(phen)] anions, and three lattice waters (figure S7). There are two crystallographically independent Ni^{2+}, which exhibit similar coordination. Different from **1** and **2**, Ni in **3** is coordinated by six nitrogens from two bim and one phen. Ni(1)–N distances are 2.083(4)–2.131(4) Å and the N–Ni–N bond angles are 78.61(15)–169.22(17)°. In the polyhedral and ball–stick representation of **3**, there exist hydrogen bonds (table S1). In **3**, the Strandberg anion $[P_2Mo_5O_{23}]$ and [Ni(bim)(Hbim)(phen)] are linked by supramolecular interactions (C10···O25 3.098, C1···O26 3.413, and C2···O15 3.358) and hydrogen bonds (O13···O19 3.005(11), O13···O6 2.868(11), and O13···O7 2.692(12)), generating a 1-D chain (figure S8). Adjacent chains are supported by weak interaction to extend to 2-D layers (figure 4). The 3-D supramolecular framework (figure S9) was generated by hydrogen bonds (O10···O17 2.785(11) and O10···O1 2.805 (12)) between terminal O of polyoxoanions from different 2-D layers. **3** represents the first supramolecular example of integrating {Ni(II)$(bim)_2$(phen)} segments with Strandberg-type phosphomolybdate.

For **1–3**, the 3-D supramolecular structures were formed by Ni(II) and water via extensive hydrogen bonds and supramolecular interactions. This indicates that the free Ni(II) complex plays an important role in the open supramolecular framework during assembly. Compared to $[CuL]_2[H_2Mo_5P_2O_{23}]\cdot 2H_2O\cdot 2CH_3CN$ and $[NiL]_2[H_2Mo_5P_2O_{23}]\cdot 10H_2O$ [38], **1–3** show 3-D supramolecular networks constructed from weak interactions among free Ni (II) complex, water, and oxygens of $[P_2Mo_5O_{23}]^{6-}$, while sandwich-type structure in the reported compounds are based on clusters of $[H_2Mo_5P_2O_{23}]^{4-}$ bridging macrocyclic metal complexes $[CuL]^{2+}$ and $[NiL]^{2+}$ to form 1-D chains and 3-D framework, respectively, via covalent bonds.

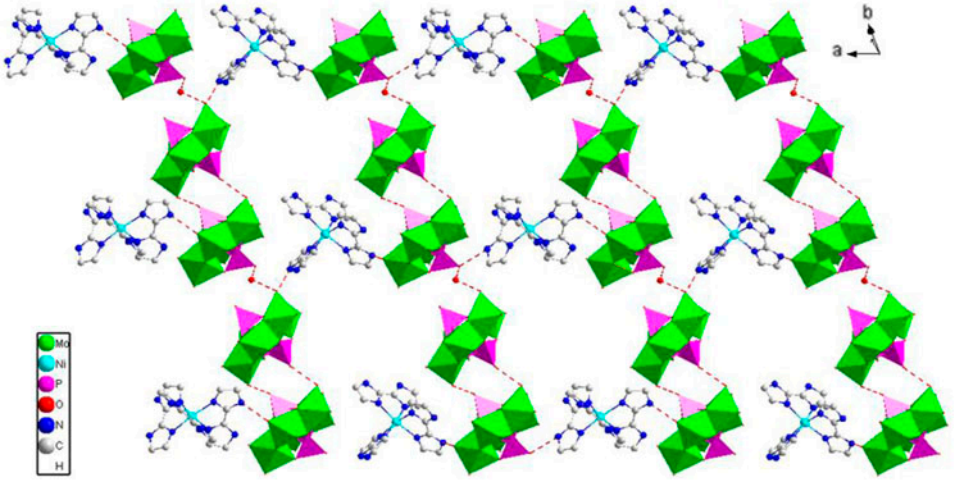

Figure 3. Polyhedral and ball–stick representation of the 2-D layers in **2**.

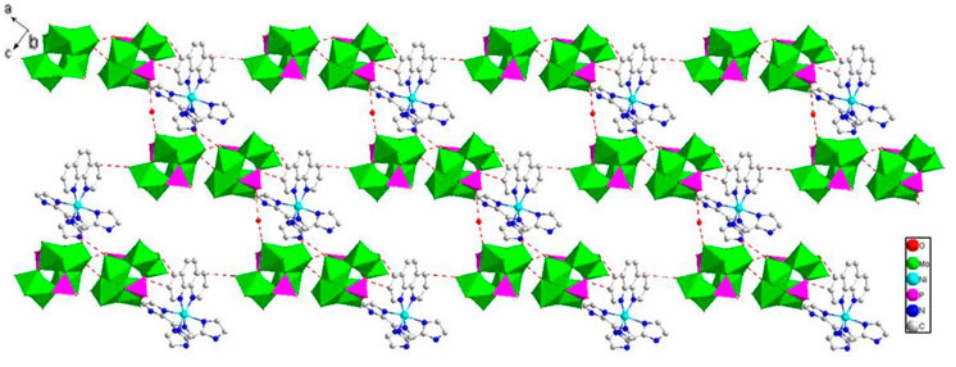

Figure 4. Polyhedral and ball–stick representation of the 2-D layers in **3**.

3.2. *IR spectrum*

IR spectra of **1**, **2,** and **3** (figure S10) exhibit the typical bands of the Strandberg-type anions from 600 to 1106 cm^{-1}. Characteristic bands at 686, 763, 901, 984, 1043, and 1103 cm^{-1} for **1**, 606, 671, 708, 795, 801, 845, 907, 925, 994, 1053, and 1107 cm^{-1} for **2,** and 603, 710, 800, 870, 953, and 1054 cm^{-1} for **3** correspond to ν(Mo–Oc–Mo), ν(Mo–Ob–Mo), ν(Mo=Od), and ν(P–O) of the P_2Mo_5 polyanions, respectively. Absorptions at 1625–1179 cm^{-1} for **1** and 1613–1213 cm^{-1} for **2** are associated with bim. Absorptions at 1603–1144 cm^{-1} for **3** are attributed to bim and 1,10-phen. IR spectra exhibit broad bands at 3451 cm^{-1} for **1**, 3446 cm^{-1} for **2,** and 3445 cm^{-1} for **3** due to the O–H stretch of water [39].

3.3. *Thermogravimetric analysis*

TG experiments were performed under N_2 at heating of 10 °C min^{-1} from 30 to 800 °C (figure S11). For **1**, TG curve displays three-step weight losses. The first of 1.89% at 126–156 °C corresponds to elimination of lattice water, calculated 1.52%, the second weight loss (38.89%) from 304 to 468 °C, and third weight loss (13.96%) from 468 to 586 °C correspond to bim and partial loss of phosphorus oxide (Calcd: 52.33%). For **2**, TG curve displays three weight loss processes. The first of 1.49% at 156–176 °C corresponds to elimination of lattice water, which is in accord with the calculated value of 1.46%, the second weight loss (24.68%) from 221 to 564 °C, and third weight loss (19.23%) from 564 to 649 °C correspond to bim ligands and the partial decomposition of the polyoxoanion framework (Calcd: 43.56%). Because the interactions of **1** and **2** are different, the weight loss processes are different. For **3**, TG curve displays two weight loss processes. The first of 3.12% at 106–245 °C corresponds to elimination of lattice water, calculated 3.09%. The second weight loss (22.94%) from 402 to 586 °C corresponds to bim and phen (Calcd: 22.9%). These results further confirm the formulas of **1–3**.

3.4. *Voltammetric behavior*

The electrochemical behaviors of **1–3** were investigated with **1**–**3**-modified CPE (**1**–**3**–CPE). The cyclic voltammetric behaviors of **1**–**3**-CPE in 1 M H_2SO_4 solution at different scan rates were recorded from –0.8 to 1.0 V for **1**-CPE and **2**-CPE, and –1.0 to 1.0 V for **3**–CPE

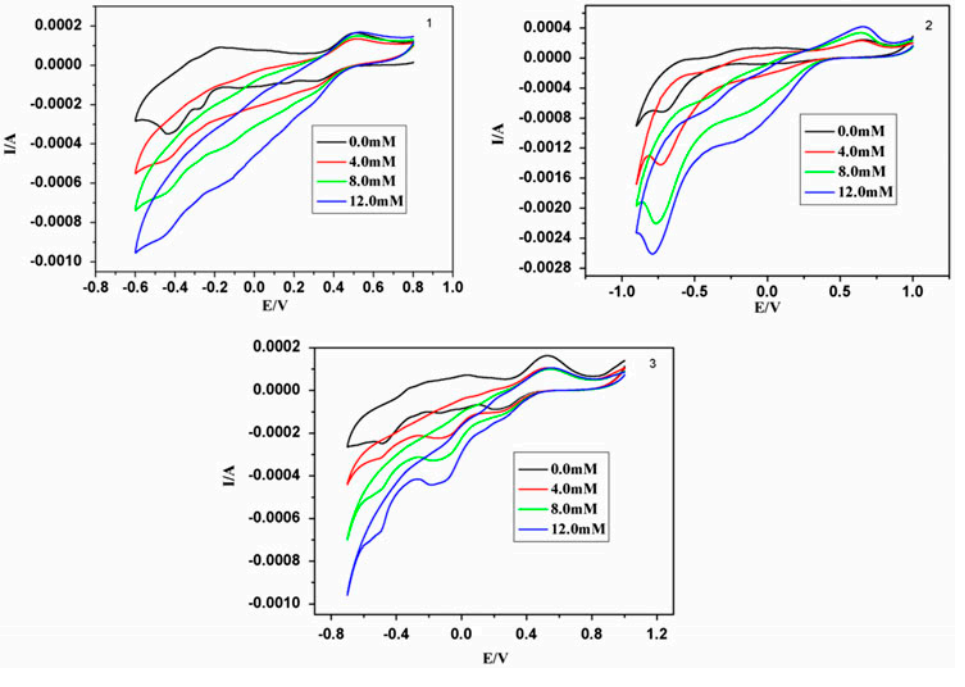

Figure 5. Cyclic voltammograms of the **1**-CPE, **2**-CPE, and **3**-CPE in 1 M H_2SO_4 solution containing 0.0, 4.0, 8.0, and 12.0 mM H_2O_2. Scan rate: 50 mV s^{-1}.

(figure S12). There exist three reversible redox peaks of I–I′, II–II′, and III–III′ with the half-wave potentials $E_{1/2}$ = (Epa + Epc)/2 (scan rate: 20 m Vs^{-1}) at –294(I–I′), –86(II–II′), and +385(III–III′) mV for **1**–CPE, –640(I–I′), –17(II–II′), and +659(III–III′) mV for **2**–CPE, and –372(I–I′), –52(II–II′), and +392(III–III′) mV for **3**-CPE, respectively, ascribed to three consecutive two-electron processes of Mo [40, 41]. The peak potentials vary gradually when the scan rate increased from 20 to 320 mV s^{-1}; the cathodic peak potentials shift to the negative direction and the corresponding anodic peak potentials to the positive direction. Peak-to-peak separation between the corresponding cathodic and anodic peaks increased, but the average peak potentials did not change.

3.5. *Electrocatalytic activity*

1–**3**-CPEs display good electrocatalytic activity on the reduction of H_2O_2 (figure 5). At the **1**-CPE, **2**-CPE, and **3**-CPE, with the addition of H_2O_2, all three reduction peak currents increased while the corresponding oxidation peak currents dramatically decreased, suggesting that H_2O_2 is reduced by two-, four-, and six-electron reduced $\{P_2Mo_5\}$ anions. The results indicate that **1**-, **2**-, and **3**-CPEs have good electrocatalytic activity towards reduction of H_2O_2.

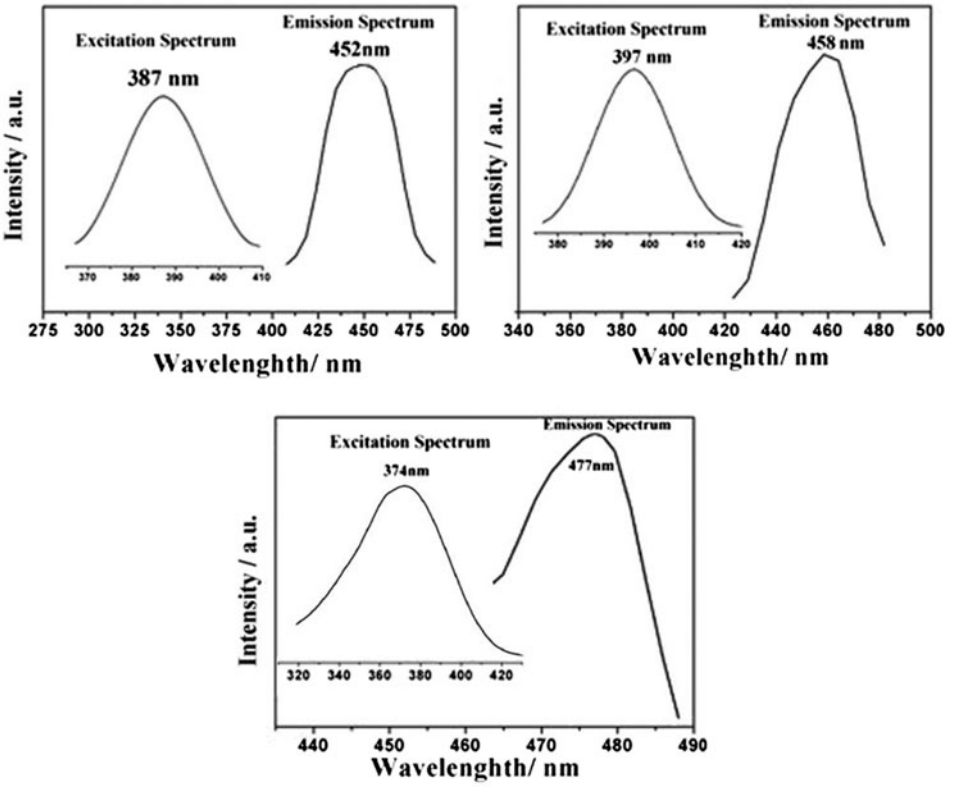

Figure 6. Fluorescent properties of **1**, **2**, and **3** in the solid state at room temperature.

3.6. *Fluorescent properties*

Emission spectra of **1**, **2**, and **3** in the solid state at room temperature were investigated (figure 6). Three prominent emission peaks were observed at 452 nm ($\lambda_{ex} = 387$ nm) for **1**, 458 nm ($\lambda_{ex} = 397$ nm) for **2**, and 477 nm ($\lambda_{ex} = 374$ nm) for **3**, similar to the emission band of bim with a maximum wavelength of 436 nm ($\lambda_{ex} = 335$ nm) [42]. For **3** containing two kinds of ligands, 1,10-phen also influences the luminescence. The emission peak can be assigned to photoluminescence of ligand-to-metal charge transfer and/or the intra ligand (π^*–π) fluorescent emission. These observations indicate that **1**, **2**, and **3** may be candidates for photoluminescence materials.

4. Conclusion

We have prepared and structurally characterized three new supramolecular compounds based on Strandberg-type $[P_2Mo_5O_{23}]^{6-}$ and Ni(II) complexes. In **1–3**, Strandberg-type POM ($[P_2Mo_5O_{23}]^{6-}$) joined to Ni(II) complex and water via hydrogen bonds and supramolecular interactions to form supramolecular frameworks from one to three dimensions. Synthesis of the compounds provides a new model for construction of POM-based supramolecular compounds. Fluorescent analysis exhibits that **1–3** are potential fluorescent materials. Electrochemical analysis shows that **1–3**-CPEs display redox properties and good electrocatalytic activity for H_2O_2.

Supplementary material

CCDC 937461, 937460, and CSD 937462 contain the supplementary crystallographic data for **1**–**3**, respectively. These data can be obtained free of charge from The Cambridge Crystallographic Data Centre via www.ccdc.cam.ac.uk/data_request/cif.

Funding

This work is supported by the National Natural Science Foundation of China [grant number 21271056], [grant number 21371042]; Specialized Research Fund for the Doctoral Program of Higher Education [grant number 20122329110001]; the Natural Science Foundation of Heilongjiang Province [grant number B201216]; Doctoral Initiation Foundation of Harbin Normal University [grant number KGB201214]; and Key Laboratory of Functional Inorganic Material Chemistry (Heilongjiang University); Ministry of Education; Program for Scientific and Technological Innovation Team Construction in Universities of Heilongjiang Province [grant number 2011TD010].

References

[1] Q. Deng, Y.L. Huang, Z.S. Peng, Z.G. Dai, M.R. Lin, T.J. Cai. *J. Solid State Chem.*, **200**, 60 (2013).
[2] J. Guo, J. Yang, Y.Y. Liu, J.F. Ma. *Inorg. Chim. Acta*, **400**, 51 (2013).
[3] M. Mannini, F. Pineider, P. Sainctavit, C. Danieli, E. Otero, C. Sciancalepore, A.M. Talarico, M.A. Arrio, A. Cornia, D. Gatteschi, R. Sessoli. *Nat. Mater.*, **8**, 194 (2009).

[4] C.H. Zhan, M.X. Jiang, Y.L. Feng, Y.H. He. *Polyhedron*, **29**, 2250 (2010).
[5] Y.H. He, Y.L. Feng, Y.Z. Lan, Y.H. Wen. *Cryst. Growth Des.*, **8**, 3586 (2008).
[6] G.Z. Li, C. Salim, H. Hinode. *Solid State Sci.*, **10**, 121 (2008).
[7] Y. Lu, J. Lü, E.B. Wang, Y.Q. Guo, X.X. Xu, L. Xu. *J. Mol. Struct.*, **740**, 159 (2005).
[8] J.B. Weng, M.C. Hong, Y.C. Liang, Q. Shi, R. Cao. *J. Chem. Soc., Dalton Trans.*, 289 (2002).
[9] Y. Lu, Y.G. Li, E.B. Wang, J. Lü, L. Xu, R. Clérac. *Eur. J. Inorg. Chem.*, **7**, 1239 (2005).
[10] X. Lu, X. Wang, P. Li, X. Pei, C. Ye. *J. Mol. Struct.*, **872**, 129 (2008).
[11] R. Cao, S. Liu, J. Cao, L. Wang, Q. Tang, Y. Liu, Y. Ren. *J. Mol. Struct.*, **888**, 307 (2008).
[12] J. Wang, J. Wang, P. Ma, J. Niu. *Chem. Lett.*, **37**, 1130 (2008).
[13] X.Y. Wu, X.F. Kuang, R.M. Yu, C.Z. Lu. *Chin. J. Struct. Chem.*, **28**, 1513 (2009).
[14] L. Wu, H. Ma, Z. Han, C. Li. *Solid State Sci.*, **11**, 43 (2009).
[15] R.C. Finn, R.S. Rarig, J. Zubieta. *Inorg. Chem.*, **41**, 2109 (2002).
[16] M.L. Qi, K. Yu, Z.H. Su, C.X. Wang, C.M. Wang, B.B. Zhou, C.C. Zhu. *Dalton Trans.*, 7586 (2013).
[17] J.B. Weng, M.C. Hong, Y.C. Liang, Q. Shi, R.J. Cao. *J. Chem. Soc., Dalton Trans.*, 289, (2002).
[18] Y. Lu, Y.G. Li, E.B. Wang. *Eur. J. Inorg. Chem.*, 1239 (2005).
[19] Y.P. Chen, H.H. Zhang, C.G. Huang. *Spectrochim. Acta, Part A*, **63**, 536 (2006).
[20] J. Thomas, A. Ramanan. *Cryst. Growth Des.*, **8**, 3390 (2008).
[21] L.H. Wu, H.Y. Ma, Z.G. Han. *Solid State Sci.*, **11**, 43 (2009).
[22] H.J. Jin, B.B. Zhou, Y. Yu, Z.F. Zhao, Z.H. Su. *CrystEngComm.*, **13**, 585 (2010).
[23] X.S. Qu, L. Xu, Y.Y. Yang, F.Y. Li, W.H. Guo. *Struct. Chem.*, **22**, 965 (2011).
[24] Y. Yu, K. Yu, B.B. Zhou, Z.F. Zhao, Z.H. Su. *Chin. J. Struct. Chem.*, **29**, 1505 (2010).
[25] M. Wei, H. Li, G. He. *J. Coord. Chem.*, **64**, 4318 (2011).
[26] J. Wu, C. Wang, K. Yu, Z. Su, Y. Yu, Y. Xu, B. Zhou. *J. Coord. Chem.*, **65**, 69 (2012).
[27] A.X. Tian, X.L. Lin, Y.J. Liu, G.Y. Liu, J. Ying, X.L. Wang, H.Y. Lin. *J. Coord. Chem.*, **65**, 2147 (2012).
[28] R. Yang, S.X. Liu, Q. Tang, S.J. Li, D.D. Liang. *J. Coord. Chem.*, **65**, 891 (2012).
[29] Z.H. Yi, X. Zhang, X.Y. Yu, L. Liu, X.Z. Xu, X.B. Cui, J.Q. Xu. *J. Coord. Chem.*, **66**, 1876 (2013).
[30] Y.L. Liu, Z.Q. Wang, X. Zhang. *Chem. Soc. Rev.*, **41**, 5922 (2012).
[31] X.S. Qu, L. Xu, Y.Y. Yang, F.Y. Li, W.H. Guo. *Struct. Chem.*, **22**, 965 (2011).
[32] C.S. Lai, F. Mohr, E.R.T. Tiekink. *CrystEngComm.*, **8**, 909 (2006).
[33] W. Kan, J. Yang, Y. Liu, J. Ma. *Polyhedron*, **30**, 2106 (2011).
[34] Y. Wang, L.C. Zhang, Z.M. Zhu, N. Li, A.F. Deng, S.Y. Zheng. *Transition Met. Chem.*, **36**, 261 (2011).
[35] M.L. Qi, K. Yu, Z.H. Su, C.X. Wang, C.M. Wang, B.B. Zhou, C.C. Zhu. *Inorg. Chem. Commun.*, **30**, 173 (2013).
[36] G.M. Sheldrick. *SHELXL 97, Program for Crystal Structure Refinement*, University of Gőttingen, Germany (1997).
[37] G.M. Sheldrick. *SHELXL 97, Program for Crystal Structure Solution*, University of Gőttingen, Germany (1997).
[38] G.C. Ou, X.Y. Yuan, Z.Z. Li, M.H. Ding. *J. Coord. Chem.*, **66**, 2065 (2013).
[39] Y. Yu, K. Yu, B.B. Zhou, Z.F. Zhao, Z.H. Su. *Chin. J. Struct. Chem.*, **29**, 1505 (2010).
[40] K. Unoura, N. Tanaka. *Inorg. Chem.*, **22**, 2963 (1983).
[41] H. Fu, W.L. Chen, E.B. Wang, J. Liu, S. Chang. *Inorg. Chim. Acta*, **362**, 1412 (2009).
[42] Z.Q. Hu, X.Z. Ye, X.G. Song, S.M. Lan. *Chin. J. Inorg. Chem.*, **27**, 1993 (2011).